

1

[ATLAS Semivisible Jets]

2

[Elena Laura Busch]

3

Submitted in partial fulfillment of the
requirements for the degree of
Doctor of Philosophy
under the Executive Committee
of the Graduate School of Arts and Sciences

4

5

6

7

8

COLUMBIA UNIVERSITY

9

2024

10

© 2024

11

[Elena Laura Busch]

12

All Rights Reserved

13

Abstract

14

[ATLAS Semivisible Jets]

15

[Elena Laura Busch]

16

Abstract of dissertation (place-holder).

Table of Contents

18	Acknowledgments	v
19	Dedication	vi
20	Introduction or Preface	1
21	Chapter 1: The Standard Model	2
22	Chapter 2: The Large Hadron Collider	4
23	2.1 LHC Timeline	4
24	2.2 Accelerator Physics	5
25	2.2.1 The Journey of a Proton	5
26	2.2.2 Magnets	7
27	2.3 Luminosity	8
28	Chapter 3: The ATLAS Detector	10
29	3.1 Coordinate System and Geometry	10
30	3.2 Inner Detector	12
31	3.2.1 Pixel Detector	12
32	3.2.2 Semiconductor Tracker	13
33	3.2.3 Transition Radiation Tracker	13

34	3.3 Calorimeters	14
35	3.3.1 Liquid Argon Calorimeter	15
36	3.3.2 Tile Calorimeter	18
37	3.4 Muon Spectrometer	19
38	3.5 Magnet System	21
39	Conclusion or Epilogue	23
40	References	27
41	Appendix A: Experimental Equipment	29
42	Appendix B: Data Processing	30

List of Figures

44	2.1 Timeline of LHC activities [9]	5
45	2.2 The LHC accelerator complex at CERN [11]	6
46	2.3 The octants of the LHC and location of various beam activities [10]	8
47	3.1 ATLAS coordinate system and geometry	12
48	3.2 A 3D visualization of the structure of the ID in the barrel region [13]	13
49	3.3 ATLAS calorimetery system [14]	14
50	3.4 Diagram of a segment of the EMB, demonstrating the accordion plate arrangement [15]	16
51		
52	3.5 A LAr pulse as produced in the detector (triangle) and after shaping (curve) [15] . .	17
53	3.6 Readout gap structure in HEC [15]	17
54	3.7 TileCal wedge module [18]	19
55	3.8 Cross section view of the muon spectrometer system [19]	20
56	3.9 Layout of the barrel and endcap toroid magnets [22]	22

List of Tables

58

Acknowledgements

59 Insert your acknowledgements text here. This page is optional, you may delete it if not
60 needed.

61

Dedication

62

Dedicated to my friends and family

63

Introduction or Preface

64 Insert your preface text here if applicable. This page is optional, you may delete it if not
65 needed. If you delete this page make sure to move page counter comment in thesis.tex to correct
66 location.

67

68

Chapter 1: The Standard Model

69 Four fundamental forces

70 The Standard Model is a universally accepted framework which explains most of the interactions
71 of fundamental particles. The SM is a renormalizable quantum field theory that obeys the local symmetry G_{SM} :

$$G_{SM} = SU(3)_C \times SU(2)_L \times U(1)_Y \quad (1.1)$$

73 The $SU(3)_C$ symmetry component is the non-Abelian gauge group of quantum chromodynamics (QCD), the theory of strong interactions. There are 8 generators for the $SU_C(3)$ group which correspond to *gluons*, massless spin-1 gauge boson which carry the force of the strong interaction.

74 75

76 Gluon and quarks, the particles which interact with the strong force, carry a color charge C .

77 The $SU(2)_L \times U(1)_Y$ symmetry group represents the electroweak sector of the Standard Model.
78 There are 4 generators for this group, which correspond to the four massless gauge bosons W^1 , W^2 ,
79 W^3 , and B. From these massless gauge bosons are formed the massive mediators of the weak force,
80 the W^- , W^+ and Z^0 bosons, and the massless electromagnetic force carrier, the photon γ .

81 The interplay between the fermionic and bosonic fields that emerge from the G_{SM} symmetry
82 can be described through the Lagrangian in equation 1.2

$$\mathcal{L} = \mathcal{L}_{kin} + \mathcal{L}_\psi + \mathcal{L}_{Yuk} + \mathcal{L}_\phi \quad (1.2)$$

83 Each term in this Lagrangian describes a set of specific particle physics interactions. \mathcal{L}_{kin}
84 . with three families of quarks and leptons, and a scalar Higgs doublet. The standard model
85 has 12 gauge bosons: 8 gluons, 3 weak bosons, and the photon. [1]

86 The physics of the Standard Model of particle physics (SM) is summarized by the SM La-
87 grangian:

$$\mathcal{L}_{kin} = -\frac{1}{4}F_{\mu\nu}F^{\mu\nu} \quad (1.3)$$

- 88 Explain equation
- 89 Explain phenomonolyg

90

91

Chapter 2: The Large Hadron Collider

92 The Large Hadron Collider (LHC) is a 26.7km circular high-energy particle accelerator, span-
93 ning the Swiss-French border near the city of Geneva, Switzerland [2]. The LHC occupies the
94 tunnel constructed in 1989 for the Large Electron-Positron (LEP) Collider, and reaches a maxi-
95 mum depth of 170m below the surface. The LHC is operated by the European Organization for
96 Nuclear Research (CERN), the largest international scientific collaboration in the world.

97

98 The LHC accelerates protons and heavy ions and collides them at four interaction points around
99 the ring, with a design center-of-mass energy per collision of $\sqrt{s} = 14$ TeV. Each interaction point
100 is home to one of four detector experiments, which study the products of the collisions. The largest
101 of these experiments is the ATLAS detector, a general purpose detector designed to study the Stan-
102 dard Model and search for new physics that could be produced in LHC collisions [3]. The CMS
103 detector is another general purpose detector, designed and operated independently of the ATLAS
104 detector, but intended to probe the same range of physics [4]. The ALICE experiment is a dedi-
105 cated heavy ion experiment, and the LHC-b experiment is a dedicated *b*-physics experiment [5] [6].

106

107 **2.1 LHC Timeline**

108 The first proton-proton collisions at the LHC were achieved in 2010 with a center-of-mass
109 energy of $\sqrt{s} = 7$ TeV. Run 1 of the LHC took place between 2010 and 2013. The data collected
110 during this time led to the discovery of the Higgs Boston in 2012 [7]. Between 2013 and 2015
111 the LHC underwent the first Long Shutdown (LS1) during which time key upgrades to the physics
112 detectors and the accelerator chain were installed. Run 2 of the LHC took place from 2015 to 2018



Figure 2.1: Timeline of LHC activities [9]

and achieved a center-of-mass energy of $\sqrt{s} = 13$ TeV. Between 2018 and 2022 the LHC underwent its second Long Shutdown (LS2). Run-3 of the LHC began in 2022 and achieved a center-of-mass energy of $\sqrt{s} = 13.6$ TeV. Run-3 is scheduled to continue through 2026, at which point the LHC machine and detectors will undergo upgrades for the *high luminosity* LHC (HL-LHC), which will increase the number of collisions by a factor of 5-10 with respect to the nominal LHC design [8].

2.2 Accelerator Physics

2.2.1 The Journey of a Proton

Protons which feed the LHC start as hydrogen gas. The electrons are removed from the hydrogen atoms through the use of strong electric fields. The linear accelerator (LINAC) then accelerates the H^- ions to an energy of 50 MeV. From here the H^- ions enter the Proton Synchrotron booster, where they are accelerated up to 1.4 GeV of energy. Subsequently they are sorted into bunches separated in time by 25 ns, where each bunch contains approximately 10^{11} protons. Next the bunches pass through the Proton Synchrotron (PS) and the Super Proton Synchrotron (SPS), where they reach energies of 25 GeV and 450 GeV respectively. Finally they are injected into the LHC as two

The CERN accelerator complex Complexe des accélérateurs du CERN

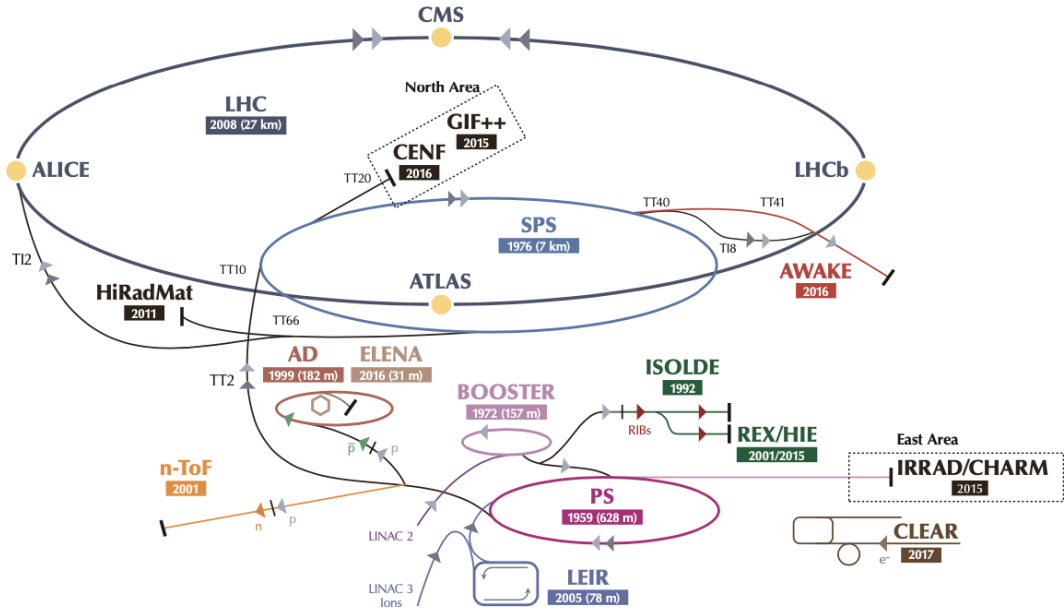


Figure 2.2: The LHC accelerator complex at CERN [11]

beams traveling in opposite direction. The original design allowed each beam to be accelerated up to 7 TeV of energy. Due to limitations with the magnet training, the highest energy actually achieved by the LHC beams during Run 2 was 6.5 TeV, giving a collision center-of-mass energy of $\sqrt{s} = 13$ TeV [10]. Figure 2.2 shows the full LHC accelerator complex.

132

Acceleration in the LHC is performed by eight radio frequency (RF) cavities located around the ring. Each RF cavity produces a 2MV electric field oscillating at 40 MHz. The 40MHz oscillation produces a point of stable equilibrium every 2.5ns. These points of equilibrium are synchronized with the occurrence of the proton bunches produced in the PS – a proton bunch occupies one out of every ten points of stable equilibrium, such that the bunches maintain a 25ns spacing [10].

138

139 2.2.2 Magnets

140 In addition to the acceleration cavities, the LHC houses 9593 superconducting magnets which
141 direct and focus the proton beam on its 27 kilometer journey. The magnets are comprised of super-
142 conducting Niobium-Titanium coils cooled to 1.9K by superfluid helium. As the beams approach
143 one of the four collision points around the ring, multipole magnets focus and squeeze the beam for
144 optimal collisions [10].

145 The LHC is divided into sections, where each section contains an a smoothly curving *arc* and
146 a straight *insertion*. The arcs are composed of 1232 large dipole magnets which bend the beam
147 to follow the roughly circular 27 km path. The main dipoles generate powerful 8.3 tesla magnetic
148 fields to achieve this bend. Each dipole magnet is 15 meters long and weighs 35 tonnes. The
149 dipoles work in conjunction with quadrupole magnets, which keep the particles in a focused beam,
150 and smaller sextupole, octupole and decapole magnets which tune the magnetic field at the ends of
151 the dipole magnets [12].

152 The straight insertion sections have different purposes depending on their location around the
153 ring: beam collisions, beam injection, beam dumping, or beam cleaning. At the four collision
154 points, insertion magnets squeeze the beam to ensure a highly focused collision. This is accom-
155 plished with a triplet of quadrupole magnets, which tighten the beam from 0.2 millimeters to just
156 16 micrometers in diameter. Insertion magnets also clean the beam, which prevents stray particles
157 from hitting sensitive components throughout the LHC. When the LHC is ready to dispose of a
158 beam of particles, beam dump magnets deflect the path of the beam into a straight line towards
159 a block of concrete and graphite that stops the beam. A dilution magnet then reduces the beam
160 intensity by a factor of 100,000 before the final stop [12]. Figure 2.3 shows the locations various
161 beam activities.

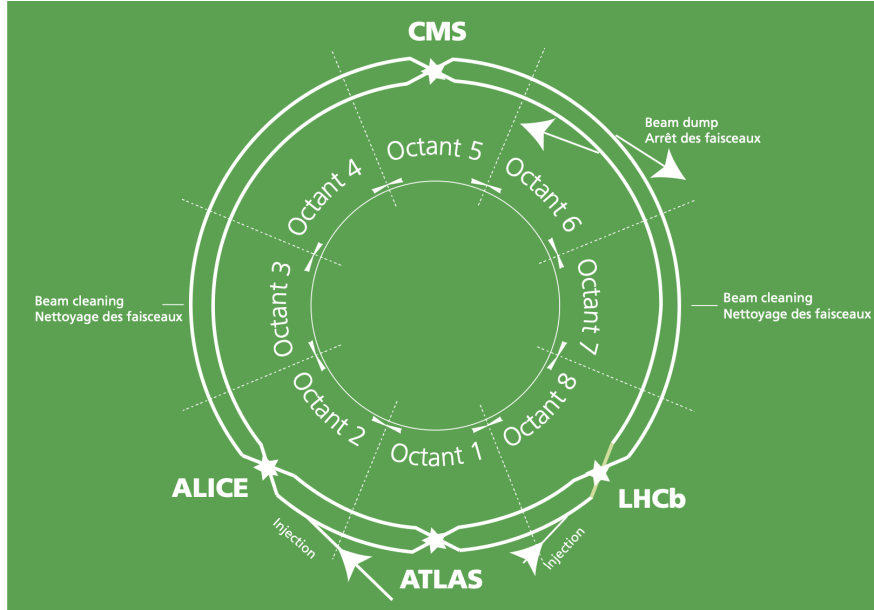


Figure 2.3: The octants of the LHC and location of various beam activities [10]

¹⁶² 2.3 Luminosity

¹⁶³ Collisions at the LHC occur when the two beams of proton bunches cross at one of the four
¹⁶⁴ interaction points. The intensity of collisions is described by the instantaneous luminosity, the
¹⁶⁵ formula for which is given in equation 2.1.

$$L = \frac{f N_1 N_2}{4\pi \sigma_x \sigma_y} \quad (2.1)$$

¹⁶⁶ Here f is the revolution frequency, N_1 and N_2 are the number of particle per bunch for each
¹⁶⁷ beam, and σ_x , σ_y are the horizontal and vertical beam widths.

¹⁶⁸

¹⁶⁹ The instantaneous luminosity gives the number of the collisions that could be produced at the
¹⁷⁰ interaction point per cm^2 of cross-sectional area per second. The integrated luminosity is obtained
¹⁷¹ by integrating the instantaneous luminosity over a given block of time, and measures the total num-
¹⁷² ber of collisions which has occurred during that operation period. This is directly correlated with
¹⁷³ the size of the datasets collected by the LHC experiments.

174

175 The design peak luminosity of the LHC is $1.0 \times 10^{34} \text{ cm}^{-2}\text{s}^{-1}$. During Run 1 of the LHC the
176 peak instantaneous luminosity was $0.8 \times 10^{34} \text{ cm}^{-2}\text{s}^{-1}$. Over the course of Run 1 the LHC collected
177 a total integrated luminosity of 5.46 fb^{-1} at $\sqrt{s} = 7 \text{ TeV}$, and 22.8 fb^{-1} at $\sqrt{s} = 8 \text{ TeV}$. Following the
178 first long shutdown and upgrade phase of operations, the LHC achieved a center of mass energy
179 $\sqrt{s} = 13 \text{ TeV}$ at the beginning of Run 2 in 2015. The LHC was also able to deliver 2.0×10^{34}
180 $\text{cm}^{-2}\text{s}^{-1}$ peak instantaneous luminosity, double the design value. During LHC Run 2, from 2015-
181 2018, the LHC delivered 156 fb^{-1} of integrated luminosity for proton-proton collisions. Run 3 of
182 the LHC began in 2022, and is expected to deliver 250 fb^{-1} of integrated luminosity to the ATLAS
183 and CMS experiments by 2026 [9].

184

185 The goal of LHC physic analyses is to find and study rare events produced by interesting
186 physics processes. The cross section σ of a given process indicates the probability of that process
187 occurring given the beam conditions of the LHC. Multiplying the cross section by the integrated
188 luminosity of a dataset gives the expected number of events for that process within the dataset.

$$N_{\text{events}} = \int \sigma L(t) dt = \mathcal{L} \times \sigma \quad (2.2)$$

189 The cross section for most processes of interest, especially BSM processes, is several orders of
190 magnitude below the total cross section for the LHC. Therefore maximizing the number of events
191 produced in collisions is crucial to increase the likelihood of producing events from processes of
192 interest. For this reason, maximizing instantaneous luminosity is a key factor in accelerator design
193 and operation.

194

195

Chapter 3: The ATLAS Detector

196 The ATLAS detector is one of two general purpose physics detectors designed to study the
197 products of the proton-proton collisions produced by the LHC. The detectors is composed of a
198 variety of specialized subsystems, designed to fully capture the large array of physics processes
199 produced in the LHC. The apparatus is 25m high, 44m in length, and weighs over 7000 tons. Colli-
200 sions occur directly in the center of the apparatus, and the cylindrical design of the detector allows
201 a complete 360 view of any physics objects resulting from the collision to be reconstructed.

202

203 Two magnet systems provide strong magnetic fields, which bend the trajectory of charged
204 particles as they pass through the magnetic fields; this allows the calculation of the momentum
205 of the particles. A 2T solenoid magnet provides a uniform magnetic field to the inner layers of
206 the detector. Further out, a toroidal magnet system (TODO: how many toroids?) provides fields
207 strengths of 0.5 to 1T

208 **3.1 Coordinate System and Geometry**

209 The ATLAS detector employs a right hand cylindrical coordinate system. The z axis is aligned
210 with the beam line, and the x-y plane sits perpendicular to the beam line. The origin is centered on
211 the detector, such that the origin corresponds with the interaction point of the two colliding beams.
212 The detector geometry is usually characterized by polar coordinates, where the azimuthal angle ϕ
213 spans the x-y plane. The polar angle θ represents the angle away from the beam line, or z axis.
214 $\theta = 0$ aligns with the positive z -axis, and $\phi = 0$ aligns with the positive x-axis.

215

216 The polar coordinate θ is generally replaced by the Lorentz invariant quantity *rapidity* y .

$$y = \frac{1}{2} \ln\left(\frac{E + p_z}{E - p_z}\right) \quad (3.1)$$

217 This substitution is advantageous because objects in the detector are traveling at highly rela-
 218 tivistic speeds. The relativistic speed of objects passing through the ATLAS detector also means
 219 that the masses of the particles are generally small compared to their total energy. In the limit of
 220 zero mass, the rapidity y reduces to the *pseudorapidity* η , which can be calculated directly from
 221 the polar angle θ .

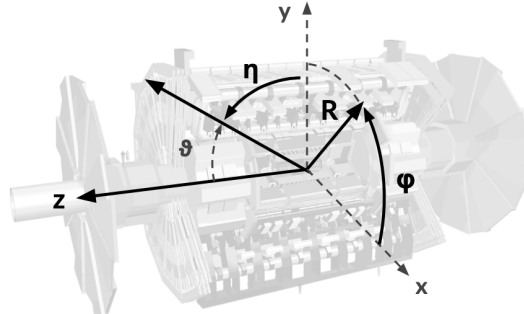
$$\eta = -\ln\left(\frac{\theta}{2}\right) \quad (3.2)$$

222 Figure 3.1a depicts the orientation of the coordinate system with respect to the ATLAS de-
 223 tector, while Figure 3.1b illustrates the relationship between θ , η , and the beamline axis z . The
 224 distance between physics objects in the detector is generally expressed in terms of the solid angle
 225 between them ΔR .

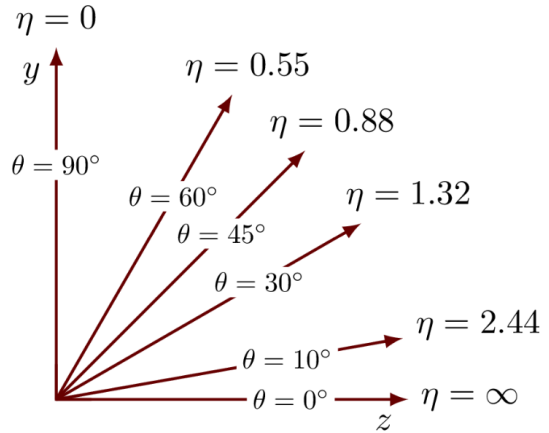
226

$$\Delta R = \sqrt{\Delta\phi^2 + \Delta\eta^2} \quad (3.3)$$

227 Head on proton-proton collisions are more likely to result in objects with a lot of energy in the
 228 transverse plane; glancing proton-proton collisions are more likely to result in objects where most
 229 of the energy is directed along the z -axis. Due to the importance of categorizing these objects,
 230 as well as the cylindrical design of the ATLAS detector, the detector is generally divided
 231 into regions in η . Each subsystem has a “central” or “barrel” region covering low $|\eta|$, while the
 232 “forward” or “endcap” regions cover $|\eta|$ up to 4.9. Each of the three main ATLAS subsystems will
 233 be discussed in the following sections.



(a) The ATLAS geometry



(b) Relationship between η and θ

Figure 3.1: ATLAS coordinate system and geometry

234 3.2 Inner Detector

235 The Inner Detector (ID) is the ATLAS subsystem closest to the interaction point. The primary
 236 purpose of the ID is to determine the charge, momentum, and trajectory of charged particles pass-
 237 ing through the detector. With this information the ID is also able to precisely determine interaction
 238 vertices.

239

240 The ID is composed of three sub-detectors; the pixel detector, the semiconductor tracker (SCT)
 241 and the transition radiation tracker (TRT). Figure 3.2 shows the location of these three subsystems
 242 with respect to each other and the interaction point.

243 3.2.1 Pixel Detector

244 The pixel detector is the first detector encountered by particles produced in LHC collisions.
 245 The original pixel detector consists of 3 barrel layers of silicon pixels, positioned at 4cm, 11cm
 246 and 14cm from the beamline. There are also 4 disks on each side positioned between 11 and 20cm,
 247 providing full coverage $|\eta| < 2.5$. The layers are comprised of silicon pixels each measuring 50
 248 μm by $300 \mu\text{m}$, with 140 million pixels in total. The pixels are organized into modules, which
 249 each contain a set of radiation hard readout electronics chips. In 2014, the Insertable B-layer

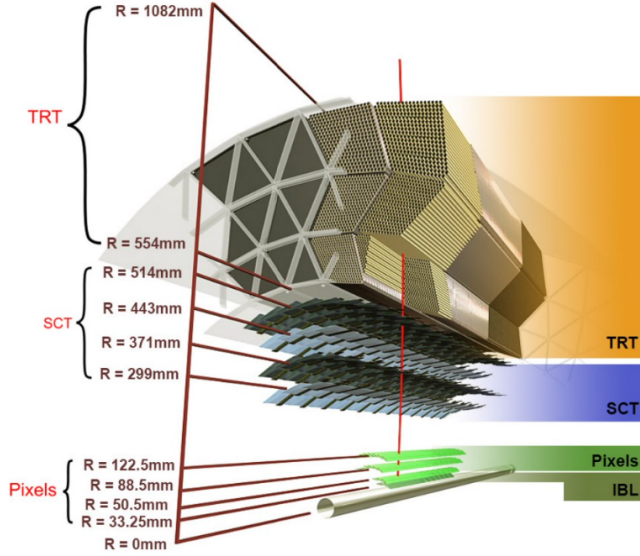


Figure 3.2: A 3D visualization of the structure of the ID in the barrel region [13]

250 (IBL) was installed, creating a new innermost layer of the pixel detector sitting just 3.3cm from the
 251 beamline. The pixels of the IBL measure $50 \mu\text{m}$ by $250 \mu\text{m}$, and cover a pseudo-rapidity range up
 252 to $|\eta| < 3$. The IBL upgrade enhances the pixel detector's ability to reconstruct secondary vertices
 253 associated with short-lived particles such as the b-quark. The improved vertex identification also
 254 helped compensate for increasing pile-up in Run 2.

255 3.2.2 Semiconductor Tracker

256 The SCT provides at least 4 additional measurements of each charged particle. It employs
 257 the same silicon technology as the Pixel Detector, but utilizes larger silicon strips which measure
 258 $80\mu\text{m}$ by 12.4cm. The SCT is composed of 4 barrel layers, located between 30cm and 52cm from
 259 the beamline, and 9 end-cap layers on each side. The SCT can distinguish tracks that are separated
 260 by at least $200\mu\text{m}$.

261 3.2.3 Transition Radiation Tracker

262 The TRT provides an additional 36 hits per particle track. The detector relies on gas filled
 263 straw tubes, a technology which is intrinsically radiation hard. The straws which are each 4mm in

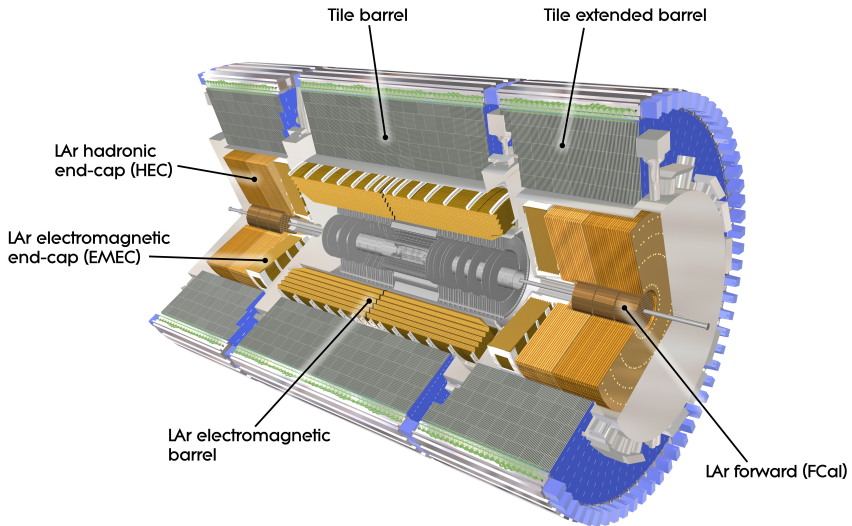


Figure 3.3: ATLAS calorimetry system [14]

264 diameter and up to 150cm in length and filled with xenon gas. The detector is composed of about
 265 50000 barrel region straws and 640000 end-cap straws, comprising 420000 electronic readout
 266 channels. Each channel provides a drift time measurement with a spatial resolution of $170\mu\text{m}$
 267 per straw. As charged particles pass through the detector and interact with the xenon, transition
 268 radiation is emitted. The use of two different drift time thresholds allows the detector to distinguish
 269 between tracking hits and transition radiation hits.

270 **3.3 Calorimeters**

271 The ATLAS calorimeter system is responsible for measuring the energy of electromagnetically
 272 and hadronically interacting particles passing through the detector. The calorimeters are located
 273 just outside the central solenoid magnet, which encloses the inner detectors. The calorimeters also
 274 stop most known particles, with the exception of muons and neutrinos, preventing them from
 275 traveling to the outermost layers of the detector. The ATLAS calorimetry system is composed of
 276 two subsystems - the Liquid Argon (LAr) calorimeter for electromagnetic calorimetry and the Tile
 277 calorimeter for hadronic calorimetry. The full calorimetry system is shown in figure 3.3.

278 3.3.1 Liquid Argon Calorimeter

279 The LAr calorimeter is a sampling calorimeter designed to trigger on and measure the energies
280 of electromagnetic particles, as well as hadronic particles in the high η regions. It is divided in sev-
281 eral regions, as shown in Figure 3.3. For the region $|\eta| < 1.4$, the electromagnetic barrel (EMB) is
282 responsible for electronic calorimetery, and provides high resolution energy, timing, and position
283 measurements for electrons and photons passing through the detector. The electromagnetic endcap
284 (EMEC) provides additional EM calorimetery up to $|\eta| < 3.2$. In the region $1.4 < |\eta| < 3.2$, the
285 hadronic endcap (HEC) provides hadronic calorimetery. For hadronic calorimetery In the region
286 $|\eta| < 1.4$, corresponding to a detector radii $> 2.2\text{m}$, the less expensive tile calorimeter (discussed
287 in the next section) is used instead. A forward calorimeter (FCAL) extends the hadronic calorime-
288 tery coverage up to $3.1 < |\eta| = 4.8$ [15].

289

290 The LAr calorimeter is composed of liquid argon sandwiched between layers of absorber mate-
291 rial and electrodes. Liquid argon is advantageous as a calorimeter active medium due to its natural
292 abundance and low cost, chemical stability, radiation tolerance, and linear response over a large
293 energy range [16]. The calorimeter is cooled to 87k by three cryostats: one barrel cryostat encom-
294 passing the EMB, and two endcap cryostats. The barrel cryostat also encloses the solenoid which
295 produces the 2T magnetic field for the inner detector. Front end electronics are housed outside the
296 cryostats and are used to process, store and transfer the calorimeter signals.

297

298 **Electromagnetic Calorimeter**

299 For the electromagnetic calorimeters, the layers of electrodes and absorber materials are ar-
300 ranged in an an accordion shape, as illustrated in Figure 3.4. The accordion shape ensures that
301 each half barrel is continuous in the azimuthal angle, which is a key feature for ensuring consistent
302 high resolution measurements. Liquid argon permeates the space between the lead absorber plates,
303 and a multilayer copper-polymide readout board runs through the center of the liquid argon filled

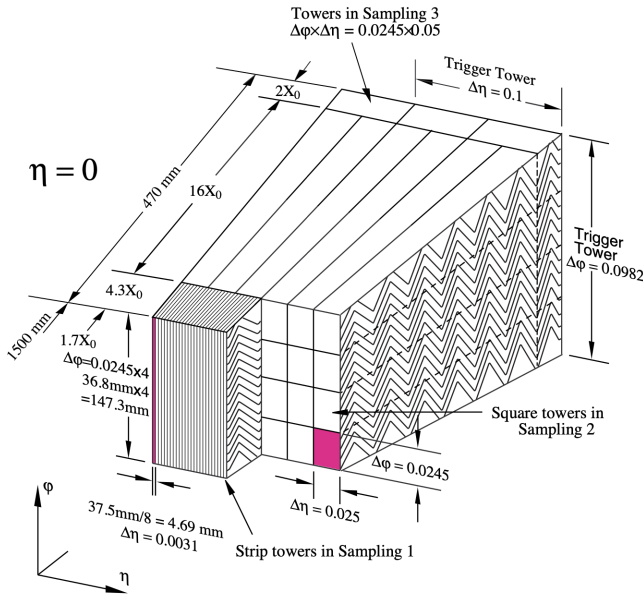


Figure 3.4: Diagram of a segment of the EMB, demonstrating the accordion plate arrangement [15]

304 gap.

305

306 The detection principle for the LAr calorimeter is the current created by electrons which are
 307 released when a charged particle ionizes the liquid argon. In the barrel region, the electrons are
 308 driven towards the center electrodes by a 2000V potential with a drift time of less than 450ns [17].

309 In the endcaps the voltage varies as a function of the radius in order to maintain a flat response [15].

310 The amount of current produced by the ionized electrons is proportional to the energy of the parti-
 311 cle creating the signal. Figure ?? shows the shape of the signal produced in the LAr calorimeter,
 312 before and after it undergoes shaping during the readout process. The shaping of the pulse enforces
 313 a positive peak and a negative tail, which ensures that subsequent pulses can be separated with
 314 the precision required for the 25ns LHC bunch spacing [15].

315

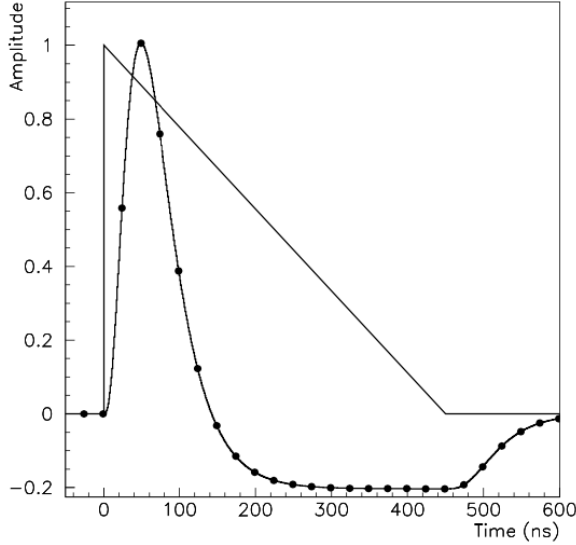


Figure 3.5: A LAr pulse as produced in the detector (triangle) and after shaping (curve) [15]

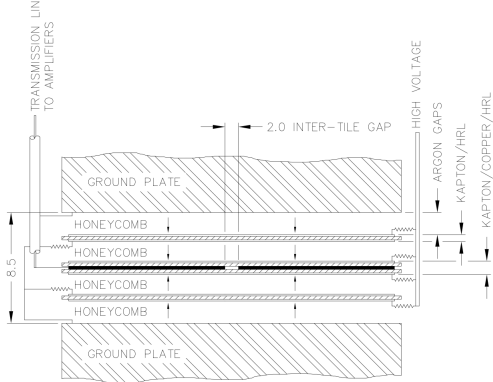


Figure 3.6: Readout gap structure in HEC [15]

316 Hadronic End-cap Calorimeter

317 The HEC sits radially beyond the EMEC. The copper absorber plates in the HEC are oriented
 318 perpendicular to the beamline, with LAr as the active medium. Each end-cap is divided into two
 319 independent wheels; the inner wheel uses 25mm copper plates, while the outer wheel uses 50mm
 320 plates as a cost saving measure. In each wheel, the 8.5mm plate gap is crossed by three parallel
 321 electrodes, creating an effective drift distance of 1.8mm. This gap is illustrated in Figure 3.6.
 322 Each wheel is divided into 32 wedge-shaped modules, each containing their own set of readout
 323 electronics.

324 **Forward Calorimeter**

325 The forward range is covered by the FCAL, which provides both EM and hadronic calorimetry.
326 It is composed of three active cylindrical modules; one EM module with copper absorber plates,
327 and two hadronic modules with tungsten absorber plates. The plates are oriented perpendicular
328 to the beamline, and LAr is used as the active material throughout. The electrodes of the FCal
329 consist of tubes that run parallel to the beam line, arranged in a honeycomb pattern. The resulting
330 LAr gaps are as small as $250 \mu\text{m}$, which enables the FCal to handle the high luminosities and the
331 resulting large influx of particles in the forward region [15].

332 3.3.2 Tile Calorimeter

333 The tile calorimeter (TileCal) provides hadronic calorimetry in the region $\eta < 1.7$, and sur-
334 rounds the LAr calorimeter. It is responsible for measurements of jet energy and jet substructure,
335 and also plays an important role in electron isolation and triggering (including muons) [18]. Tile-
336 Cal is composed of 3 sections, as shown in figure 3.3; a barrel calorimeter sits directly outside the
337 LAr EMB and provides coverage up to $\eta < 1.0$. Two extended barrel sections sit outside the LAr
338 endcaps and cover the region $0.8 < \eta < 1.7$.

339

340 TileCal is a sampling calorimeter composed of steel and plastic scintillator plates as illustrated
341 in Figure 3.7. A total of 460,000 scintillators are read out by wavelength-shifting fibers. The
342 fibers are gathered to define cells and in turn read out by photomultiplier tubes, which amplify
343 the signal and convert it to an electrical signature. Each cell has an approximate granularity of
344 $\Delta\eta \times \Delta\phi = 0.1 \times 0.1$. Each barrel is divided azimuthally into 64 independent modules, an example
345 of which is show in Figure 3.7. The modules are each serviced by front-end electronic housed in a
346 water-cooled drawer on the exterior of the module.

347

348 The detection principle of the TileCal is the production of light from hadronic particles inter-
349 acting with the scintillating tiles. When a hadronic particle hits the steel plate, a shower of particles

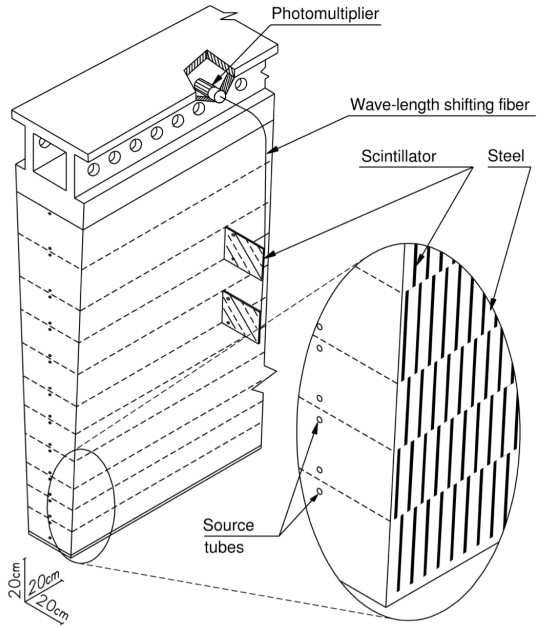


Figure 3.7: TileCal wedge module [18]

350 are produced. The interaction of the shower with the plastic scintillator produces photons, the num-
 351 ber and intensity of which are proportional to the original particle's energy.

352

353 3.4 Muon Spectrometer

354 Unlike electrons, photons, and hadrons, muons interact minimally with the ATLAS calorime-
 355 ters, and can pass through large amounts of detector material without stopping. The ATLAS muon
 356 spectrometer (MS) provides additional tracking information to improve the identification and mea-
 357 surement of muons. The MS comprises the outermost layers of the detector, and is interspersed
 358 with toroid magnets (discussed in section 3.5), which provide a magnetic field of approximately
 359 0.5T. The magnetic field bends the trajectory of the muons as they pass through the detector, and
 360 the degree of the bend is directly correlated with the muon momentum. The path of the muon
 361 is primarily measured by hits in three layers of monitored drift tube (MDT) precision chambers,
 362 which cover the range $|\eta| < 2.7$. The barrel layout of the MS is show in Figure 3.8.

363

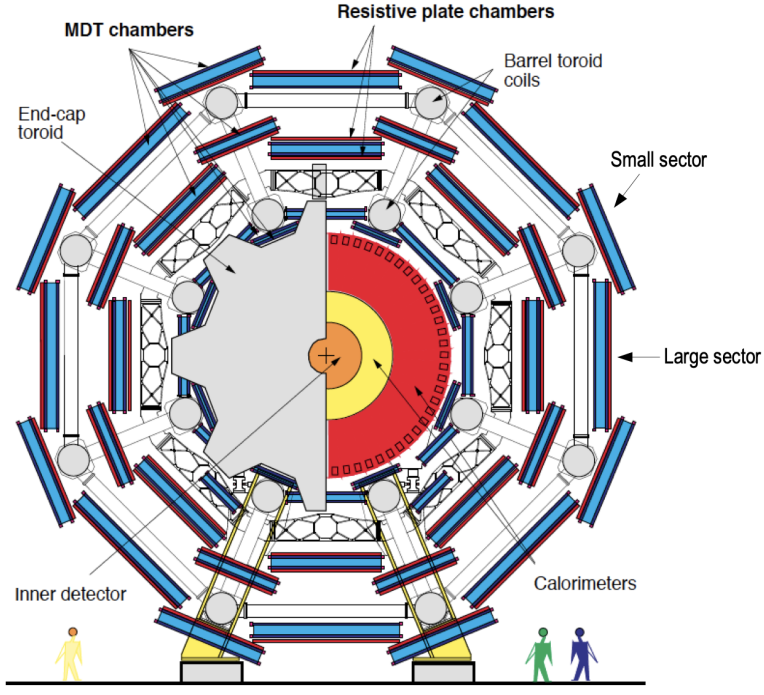


Figure 3.8: Cross section view of the muon spectrometer system [19]

364 Muon triggering is provided by three layers of resistive place chambers (RPC) in the barrel
 365 ($|\eta| < 1.05$), and 3-4 layers of thin gap chambers (TGC) in the endcaps ($1.05 < |\eta| < 2.4$). RPCs
 366 and TGCs also provide muon track measurements in the non-bending coordinate (ϕ). RPCs are
 367 constructed from two parallel resistive plates separated by a 2mm gap filled with a sensitive gas
 368 mixture. This provides a total of six independent measurements for each muon track, with a spatial
 369 resolution of 1cm and a time resolution of 1ns. Time measurements from the RPCs are primarily
 370 associated to hits in the MDT precision chambers to correct the bunch crossing. The time mea-
 371 surement is also used to reject cosmic muons, and to search for delayed signals. TCGs provide
 372 triggering in the endcap regions, and consist of parallel 30 μm wires suspended in a sensitive gas
 373 mixture. TCGs provide high radiation tolerance and a fast response time, both features that are
 374 necessary for handling the high flux of muons in the forward region [19].

375

376 Precision measurements of muon momentum and position are primarily achieved by MDTs.
 377 The MDTs are constructed from 30mm diameter tubes, permeated by a gas mixture of 93% Ar and

378 7% CO₂. The average single-tube spatial resolution is 80 μm. Each chamber consists of six drift
379 tube layers, which together provide a muon track segment resolution of 35 μm. The momentum
380 of the muons can be calculated from the bend in the muon trajectory as they pass through the
381 0.5T magnetic field provided by the toroids. For a $p_T = 1$ TeV track, the average p_T resolution is
382 11%. In the inner most endcap wheels, cathode strip chambers (CSC) are used instead of MDTs,
383 covering the region $2.0 < |\eta| < 2.7$. CSCs are multiwire proportional chambers, with a cathode
384 strip readout. The CSCs have a spatial resolution in the range of 50 μm, and a maximum drift time
385 of about 30 ns, which makes them superior for handling the high flux of particles in the forward
386 region [20].

387 **3.5 Magnet System**

388 The ATLAS magnet system consists of four sets of superconducting magnets: a barrel solenoid,
389 barrel toroid, and two endcap toroids. The solenoid magnet produces a 2T magnetic field respon-
390 sible for bending the trajectories of charged particles as they pass through the inner detector. The
391 three toroid magnets provide a field of 0.5 - 1 T and curve the path of muons passing through the
392 muon spectrometer.

393

394 The inner solenoid magnet is composed of over 9km of niobium-titanium superconductor
395 wires, which are imbedded into strengthen pure aluminum strips. The solenoid is just 4.5 cm
396 thick, which minimizes interactions between the magnet material and particles passing through the
397 detector. It is housed in the LAr cryostat, as described in section 3.3.1, which further reduces the
398 amount of non-detector material required to support the solenoid. The return yoke of the magnet
399 is provided by the iron absorber of the TileCal [21].

400

401 The central ATLAS toroid magnet, providing the magnetic field for the barrel region of the MS,
402 is the largest toroidal magnet ever constructed at 25m in length. The toroid is composed of eight
403 individual coils, each housed in their own cryostat. The toroidal magnetic field is advantageous

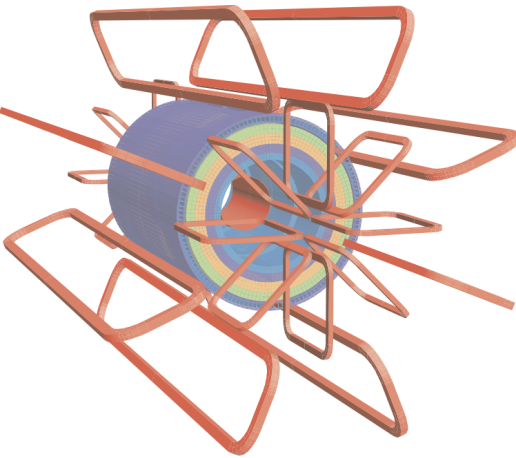


Figure 3.9: Layout of the barrel and endcap toroid magnets [22]

as the direction of the field is almost perpendicular to the path of the charged particles. 56 km of aluminum stabilized niobium-titanium-copper superconductor wire compose the magnet. In each endcap, eight smaller superconducting coils extend the toroidal magnetic field to particles leaving the detector in the forward direction [21]. Figure 3.9 shows the layout of the toroid magnets.

Conclusion or Epilogue

409 Use this page for your epilogue or conclusion if applicable; please use only one of the titles
410 for this page. Otherwise, you may delete it. Use this page for your epilogue or conclusion if
411 applicable; please use only one of the titles for this page. Otherwise, you may delete it. Use this
412 page for your epilogue or conclusion if applicable; please use only one of the titles for this page.
413 Otherwise, you may delete it. Use this page for your epilogue or conclusion if applicable; please
414 use only one of the titles for this page. Otherwise, you may delete it. Use this page for your
415 epilogue or conclusion if applicable; please use only one of the titles for this page. Otherwise,
416 you may delete it. Use this page for your epilogue or conclusion if applicable; please use only one
417 of the titles for this page. Otherwise, you may delete it. Use this page for your epilogue or
418 conclusion if applicable; please use only one of the titles for this page. Otherwise, you may delete
419 it. Use this page for your epilogue or conclusion if applicable; please use only one of the titles for
420 this page. Otherwise, you may delete it. Use this page for your epilogue or conclusion if
421 applicable; please use only one of the titles for this page. Otherwise, you may delete it. Use this
422 page for your epilogue or conclusion if applicable; please use only one of the titles for this page.
423 Otherwise, you may delete it. Use this page for your epilogue or conclusion if applicable; please
424 use only one of the titles for this page. Otherwise, you may delete it. Use this page for your
425 epilogue or conclusion if applicable; please use only one of the titles for this page. Otherwise,
426 you may delete it. Use this page for your epilogue or conclusion if applicable; please use only one
427 of the titles for this page. Otherwise, you may delete it. Use this page for your epilogue or
428 conclusion if applicable; please use only one of the titles for this page. Otherwise, you may delete

429 it. Use this page for your epilogue or conclusion if applicable; please use only one of the titles for
430 this page. Otherwise, you may delete it. Use this page for your epilogue or conclusion if
431 applicable; please use only one of the titles for this page. Otherwise, you may delete it. Use this
432 page for your epilogue or conclusion if applicable; please use only one of the titles for this page.
433 Otherwise, you may delete it. Use this page for your epilogue or conclusion if applicable; please
434 use only one of the titles for this page. Otherwise, you may delete it. Use this page for your
435 epilogue or conclusion if applicable; please use only one of the titles for this page. Otherwise,
436 you may delete it. Use this page for your epilogue or conclusion if applicable; please use only one
437 of the titles for this page. Otherwise, you may delete it. Use this page for your epilogue or
438 conclusion if applicable; please use only one of the titles for this page. Otherwise, you may delete
439 it. Use this page for your epilogue or conclusion if applicable; please use only one of the titles for
440 this page. Otherwise, you may delete it. Use this page for your epilogue or conclusion if
441 applicable; please use only one of the titles for this page. Otherwise, you may delete it. Use this
442 page for your epilogue or conclusion if applicable; please use only one of the titles for this page.
443 Otherwise, you may delete it. Use this page for your epilogue or conclusion if applicable; please
444 use only one of the titles for this page. Otherwise, you may delete it. Use this page for your
445 epilogue or conclusion if applicable; please use only one of the titles for this page. Otherwise,
446 you may delete it. Use this page for your epilogue or conclusion if applicable; please use only one
447 of the titles for this page. Otherwise, you may delete it. Use this page for your epilogue or
448 conclusion if applicable; please use only one of the titles for this page. Otherwise, you may delete
449 it. Use this page for your epilogue or conclusion if applicable; please use only one of the titles for
450 this page. Otherwise, you may delete it. Use this page for your epilogue or conclusion if
451 applicable; please use only one of the titles for this page. Otherwise, you may delete it. Use this
452 page for your epilogue or conclusion if applicable; please use only one of the titles for this page.
453 Otherwise, you may delete it. Use this page for your epilogue or conclusion if applicable; please
454 use only one of the titles for this page. Otherwise, you may delete it. Use this page for your
455 epilogue or conclusion if applicable; please use only one of the titles for this page. Otherwise,

456 you may delete it. Use this page for your epilogue or conclusion if applicable; please use only one
457 of the titles for this page. Otherwise, you may delete it. Use this page for your epilogue or
458 conclusion if applicable; please use only one of the titles for this page. Otherwise, you may delete
459 it. Use this page for your epilogue or conclusion if applicable; please use only one of the titles for
460 this page. Otherwise, you may delete it. Use this page for your epilogue or conclusion if
461 applicable; please use only one of the titles for this page. Otherwise, you may delete it. Use this
462 page for your epilogue or conclusion if applicable; please use only one of the titles for this page.
463 Otherwise, you may delete it. Use this page for your epilogue or conclusion if applicable; please
464 use only one of the titles for this page. Otherwise, you may delete it. Use this page for your
465 epilogue or conclusion if applicable; please use only one of the titles for this page. Otherwise,
466 you may delete it. Use this page for your epilogue or conclusion if applicable; please use only one
467 of the titles for this page. Otherwise, you may delete it. Use this page for your epilogue or
468 conclusion if applicable; please use only one of the titles for this page. Otherwise, you may delete
469 it. Use this page for your epilogue or conclusion if applicable; please use only one of the titles for
470 this page. Otherwise, you may delete it. Use this page for your epilogue or conclusion if
471 applicable; please use only one of the titles for this page. Otherwise, you may delete it. Use this
472 page for your epilogue or conclusion if applicable; please use only one of the titles for this page.
473 Otherwise, you may delete it. Use this page for your epilogue or conclusion if applicable; please
474 use only one of the titles for this page. Otherwise, you may delete it. Use this page for your
475 epilogue or conclusion if applicable; please use only one of the titles for this page. Otherwise,
476 you may delete it. Use this page for your epilogue or conclusion if applicable; please use only one
477 of the titles for this page. Otherwise, you may delete it. Use this page for your epilogue or
478 conclusion if applicable; please use only one of the titles for this page. Otherwise, you may delete
479 it. Use this page for your epilogue or conclusion if applicable; please use only one of the titles for
480 this page. Otherwise, you may delete it. Use this page for your epilogue or conclusion if
481 applicable; please use only one of the titles for this page. Otherwise, you may delete it. Use this
482 page for your epilogue or conclusion if applicable; please use only one of the titles for this page.

483 Otherwise, you may delete it. Use this page for your epilogue or conclusion if applicable; please
484 use only one of the titles for this page. Otherwise, you may delete it. Use this page for your
485 epilogue or conclusion if applicable; please use only one of the titles for this page. Otherwise,
486 you may delete it. Use this page for your epilogue or conclusion if applicable; please use only one
487 of the titles for this page. Otherwise, you may delete it. Use this page for your epilogue or
488 conclusion if applicable; please use only one of the titles for this page. Otherwise, you may delete
489 it. Use this page for your epilogue or conclusion if applicable; please use only one of the titles for
490 this page. Otherwise, you may delete it. Use this page for your epilogue or conclusion if
491 applicable; please use only one of the titles for this page. Otherwise, you may delete it. Use this
492 page for your epilogue or conclusion if applicable; please use only one of the titles for this page.
493 Otherwise, you may delete it. Use this page for your epilogue or conclusion if applicable; please
494 use only one of the titles for this page. Otherwise, you may delete it. Use this page for your
495 epilogue or conclusion if applicable; please use only one of the titles for this page. Otherwise,
496 you may delete it. Use this page for your epilogue or conclusion if applicable; please use only one
497 of the titles for this page. Otherwise, you may delete it. Use this page for your epilogue or
498 conclusion if applicable; please use only one of the titles for this page. Otherwise, you may delete
499 it. Use this page for your epilogue or conclusion if applicable; please use only one of the titles for
500 this page. Otherwise, you may delete it. Use this page for your epilogue or conclusion if
501 applicable; please use only one of the titles for this page. Otherwise, you may delete it. Use this
502 page for your epilogue or conclusion if applicable; please use only one of the titles for this page.
503 Otherwise, you may delete it. Use this page for your epilogue or conclusion if applicable; please
504 use only one of the titles for this page. Otherwise, you may delete it. Use this page for your
505 epilogue or conclusion if applicable; please use only one of the titles for this page. Otherwise,
506 you may delete it. Use this page for your epilogue or conclusion if applicable; please use only one
507 of the titles for this page. Otherwise, you may delete it. Use this page for your epilogue or
508 conclusion if applicable; please use only one of the titles for this page. Otherwise, you may delete
509 it.

References

- 511 [1] M. Tanabashi et al. “Review of Particle Physics”. In: *Phys. Rev. D* 98 (3 2018), pp. 847–851.
- 512 [2] Lyndon Evans and Philip Bryant. “LHC Machine”. In: *Journal of Instrumentation* 3.08
513 (2008), S08001.
- 514 [3] “The ATLAS Experiment at the CERN Large Hadron Collider”. In: *JINST* 3 (2008). Also
515 published by CERN Geneva in 2010, S08003.
- 516 [4] “The CMS experiment at the CERN LHC”. In: *Journal of Instrumentation* 3.08 (2008),
517 S08004.
- 518 [5] “The ALICE experiment at the CERN LHC”. In: *Journal of Instrumentation* 3.08 (2008),
519 S08002.
- 520 [6] “The LHCb Detector at the LHC”. In: *Journal of Instrumentation* 3.08 (2008), S08005.
- 521 [7] Aad G., et al. (ATLAS Collaboration and CMS Collaboration). “Combined Measurement of
522 the Higgs Boson Mass in pp Collisions at $\sqrt(s) = 7$ and 8 TeV with the ATLAS and CMS
523 Experiments”. In: *Phys. Rev. Lett.* 114 (19 2015), p. 191803.
- 524 [8] O. Aberle et al. *High-Luminosity Large Hadron Collider (HL-LHC): Technical design re-*
525 *port*. CERN Yellow Reports: Monographs. Geneva: CERN, 2020.
- 526 [9] *The High-Luminosity LHC*. [https://voisins.web.cern.ch/high-](https://voisins.web.cern.ch/high-luminosity-lhc-hl-lhc)
527 [luminosity-lhc-hl-lhc](https://voisins.web.cern.ch/high-luminosity-lhc-hl-lhc). Accessed: 2024-01-05.
- 528 [10] Ana Lopes and Melissa Loyse Perrey. *FAQ-LHC The guide*. 2022.
- 529 [11] Esma Mobs. “The CERN accelerator complex in 2019. Complexe des accélérateurs du
530 CERN en 2019”. In: (2019). General Photo.
- 531 [12] *Pulling together: Super Conducting electromagnets*. <https://home.cern/science/engineering/pulling-together-superconducting-electromagnets>.
532 Accessed: 2024-01-05.
- 533 [13] G Aad, B Abbott, and ATLAS Collaboration. “Performance of the reconstruction of large
534 impact parameter tracks in the inner detector of ATLAS”. In: *Eur. Phys. J. C Part. Fields*
535 83.11 (Nov. 2023).
- 536 [14] Joao Pequenao. *Computer Generated image of the ATLAS calorimeter*. 2008.

- 538 [15] *ATLAS liquid-argon calorimeter: Technical Design Report*. Technical design report. AT-
539 LAS. Geneva: CERN, 1996.
- 540 [16] H A Gordon. “Liquid argon calorimetry for the SSC”. In: () .
- 541 [17] Henric Wilkens and (on behalf ofthe ATLAS LArg Collaboration). “The ATLAS Liquid
542 Argon calorimeter: An overview”. In: *Journal of Physics: Conference Series* 160.1 (2009),
543 p. 012043.
- 544 [18] *Technical Design Report for the Phase-II Upgrade of the ATLAS Tile Calorimeter*. Tech.
545 rep. Geneva: CERN, 2017.
- 546 [19] “Technical Design Report for the Phase-II Upgrade of the ATLAS Muon Spectrometer”. In:
547 () .
- 548 [20] L Pontecorvo. “The ATLAS Muon Spectrometer”. In: (2004). revised version number 1
549 submitted on 2003-07-27 16:31:16.
- 550 [21] *ATLAS magnet system: Technical Design Report, 1*. Technical design report. ATLAS. Geneva:
551 CERN, 1997.
- 552 [22] The ATLAS Collaboration. “The ATLAS Experiment at the CERN Large Hadron Collider”.
553 In: *Journal of Instrumentation* 3.08 (2008), S08003.

Appendix A: Experimental Equipment

556 Lorem ipsum dolor sit amet, consectetur adipiscing elit, sed do eiusmod tempor incididunt ut
557 labore et dolore magna aliqua. Ut enim ad minim veniam, quis nostrud exercitation ullamco laboris
558 nisi ut aliquip ex ea commodo consequat. Duis aute irure dolor in reprehenderit in voluptate velit
559 esse cillum dolore eu fugiat nulla pariatur. Excepteur sint occaecat cupidatat non proident, sunt in
560 culpa qui officia deserunt mollit anim id est laborum.

Appendix B: Data Processing

563 Lorem ipsum dolor sit amet, consectetur adipiscing elit, sed do eiusmod tempor incididunt ut
564 labore et dolore magna aliqua. Ut enim ad minim veniam, quis nostrud exercitation ullamco laboris
565 nisi ut aliquip ex ea commodo consequat. Duis aute irure dolor in reprehenderit in voluptate velit
566 esse cillum dolore eu fugiat nulla pariatur. Excepteur sint occaecat cupidatat non proident, sunt in
567 culpa qui officia deserunt mollit anim id est laborum.